Research Square

Preprints are preliminary reports that have not undergone peer review.
They should not be considered conclusive, used to inform clinical practice,
or referenced by the media as validated information.

Integrated Bulk and Single Cell Transcriptomics Reveal That CD48 Marks an Immune Activated Microenvironment and Predicts Favorable Prognosis in Cervical Cancer

Jiajian Huang
The Affiliated Qingyuan Hospital (Qingyuan People's Hospital)
Yang Yang
yycxf0620@sina.com
The Affiliated Qingyuan Hospital (Qingyuan People's Hospital)
Qinglan Hu
The Affiliated Qingyuan Hospital (Qingyuan People's Hospital)
Xue Han
The Affiliated Qingyuan Hospital (Qingyuan People's Hospital)

Research Article

Keywords: cervical cancer, CD48, immune microenvironment, prognostic marker, multi-omics

Posted Date: November 16th, 2026

DOI: https://doi.org/10.21203/rs.3.rs-11239809/v1

License: This work is licensed under a Creative Commons Attribution 4.0 International License.
Read Full License

Additional Declarations: No competing interests reported.

Integrated Bulk and Single Cell Transcriptomics Reveal That CD48 Marks an Immune Activated Microenvironment and Predicts Favorable Prognosis in Cervical Cancer

Jiajian Huang[1,], YangYang[1]*, Hu Qinglan[1]

1 Department of Obstetrics and Gynecology, The Affiliated Qingyuan Hospital (Qingyuan People's Hospital), Guangzhou Medical University, Qingyuan, Guangdong, China, 511518

[a] These authors Contributed equally to this work.

*Corresponding authors

YangYang, Email: yycxf0620@sina.com

Abstract: Cervical cancer is driven by persistent infection with high-risk human papillomavirus (HPV), and treatment options for recurrent or metastatic disease remain limited because immune checkpoint inhibitors benefit only a subset of patients. Reliable prognostic markers are therefore still needed. Here we integrated TCGA-CESC bulk transcriptomes with the GSE168652 single-cell dataset to screen immune-related cervical cancer targets (IRCTs) through weighted gene co-expression network analysis (WGCNA), machine-learning feature selection, and survival modeling, and then characterized the expression, prognostic value, and immune-microenvironment associations of the core gene. CD48 was selected as the consensus core gene by multiple algorithms, and its high expression was associated with longer overall survival (multivariate Cox HR = 0.498, 95% CI 0.302–0.822, p = 0.006). High CD48 coincided with elevated immune scores, increased infiltration of immune effector cells, and upregulation of several immune checkpoint molecules. Single-cell analysis showed that CD48 was expressed mainly in CD8+ T cells, natural killer (NK) cells, and monocytes/macrophages, whereas epithelial or tumor cells were nearly negative. Virtual knockout further showed that loss of CD48 significantly perturbed the cytotoxic effectors NKG7 and GZMA. These findings identify CD48 as a candidate marker that reflects an immune-activated microenvironment and carries independent prognostic value in cervical cancer.

Keywords: cervical cancer; CD48; immune microenvironment; prognostic marker; multi-omics

1. Introduction

Cervical cancer arises from persistent infection with high-risk HPV and is histologically divided into squamous cell carcinoma and adenocarcinoma [1]. Surgery, radiotherapy, and chemoradiotherapy have improved outcomes for patients with early-stage disease, but overall survival in advanced, recurrent, and metastatic cases remains poor and treatment options are limited. New markers that inform both prognosis and treatment are therefore an ongoing clinical need [2].

The tumor microenvironment (TME) contributes to cervical cancer progression, immune escape, and treatment resistance [3]. Immune checkpoint inhibitors targeting the PD-1/PD-L1 axis are now approved for recurrent or metastatic cervical cancer [4, 5], yet only a proportion of patients achieve durable responses, and markers that reliably predict prognosis or identify likely responders are still lacking [5].

CD48 (also known as SLAMF2) is a glycosylphosphatidylinositol (GPI)-anchored cell-surface glycoprotein of the signaling lymphocytic activation molecule (SLAM) family and a natural ligand of the T-cell receptor CD2 [6]. It is expressed predominantly on hematopoietic and immune cells, including T cells, NK cells, B cells, monocytes/macrophages, and dendritic cells. Through CD48–CD2 interaction, CD48 delivers costimulatory signals that regulate lymphocyte activation, NK-cell cytotoxicity, and cell adhesion [6, 7]. Its expression profile, prognostic value, and influence on the immune microenvironment in cervical cancer have not been described systematically at the multi-omics level.

In this study, we integrated bulk and single-cell transcriptomes to identify CD48 as a core gene from immune-related cervical cancer targets, using WGCNA, machine-learning feature selection, and survival analysis. We then characterized its expression, prognostic significance, and effect on immune-microenvironment remodeling; mapped its cellular localization, differentiation dynamics, and cell-cell communication at single-cell resolution; assessed its association with drug sensitivity and somatic mutations; and inferred its downstream regulatory network by virtual knockout.

2. Materials and Methods

2.1 Data Sources and Preprocessing

RNA-sequencing expression data (FPKM, STAR pipeline) and corresponding clinical information for the TCGA-CESC project were obtained from The Cancer Genome Atlas (TCGA) (https://portal.gdc.cancer.gov/). Ensembl (http://asia.ensembl.org) gene identifiers were mapped to gene symbols with org.Hs.eg.db; when multiple identifiers mapped to one symbol, the maximum expression value was retained, followed by log2(FPKM + 1) transformation. Clinical information included age, FIGO stage, and histological subtype. After removing samples without survival information or without matched expression data, 296 cervical cancer samples remained. Two independent cohorts, GSE63514 and GSE39001, were downloaded from the Gene Expression Omnibus (GEO) (http://www.ncbi.nlm.nih.gov/geo/) as expression validation sets. Cervical cancer-related target genes were retrieved from the Comparative Toxicogenomics Database (CTD; 12 genes) (http://ctdbase.org/) and GeneCards (6,661

genes) (https://www.genecards.org/). The cervical cancer single-cell dataset GSE168652 (2 samples; 24,498 cells after quality control, comprising 13,104 tumor and 11,394 normal cells) was obtained for single-cell analysis.

2.2 Identification and Functional Enrichment of IRCTs

We used xCell [8] to compute the ImmuneScore of each TCGA-CESC sample. WGCNA [9] was applied to the 5,000 most variable genes to build a co-expression network; modules were defined by hierarchical clustering and dynamic tree cutting (minModuleSize = 120). Module eigengenes were correlated with ImmuneScore to identify the most relevant core module, and genes in this module were intersected with the CTD and GeneCards cervical cancer targets to obtain immune-related cervical cancer targets (IRCTs). KEGG pathway and Gene Ontology (GO) biological process enrichment analyses of IRCTs were performed with clusterProfiler.

2.3 Core Gene Selection

A co-expression network of IRCTs was constructed from the WGCNA topological overlap matrix (TOM) (threshold 0.2) and exported to Cytoscape for visualization and topology analysis. Feature selection combined three machine-learning algorithms: LASSO regression (10-fold cross-validation, lambda.1se criterion), random forest [10] (variable importance ranked by mean decrease in Gini), and SVM-RFE [11] (recursive feature elimination). Univariate Cox regression was run for each of the 364 IRCTs ($p < 0.05$), and genes significant in univariate Cox regression were intersected with the

LASSO and random forest outputs to define consensus core genes. CD48 was then selected as the core target gene.

2.4 CD48 Expression and Prognostic Analysis

The two GEO cohorts (GSE63514 and GSE39001) were used to validate CD48 expression differences between normal cervical tissue and cervical cancer tissue. In TCGA-CESC, samples were split into high and low groups at the median CD48 expression, and Kaplan-Meier analysis with the log-rank test evaluated the association between CD48 and overall survival (OS). Univariate and multivariate Cox regression (adjusting for age, FIGO stage, and histological subtype) assessed the independent prognostic value of CD48. Time-dependent ROC curves were drawn and 1-, 3-, and 5-year AUCs computed. A multi-gene risk score model was built from the four consensus core genes and its discriminative ability assessed. A nomogram predicting individual 1-, 3-, and 5-year survival probabilities was constructed with the rms package, and the associations of CD48 expression with FIGO stage and histological subtype were examined.

2.5 Tumor Immune Microenvironment Analysis

We used xCell to estimate immune cell infiltration and compared the immune-microenvironment composition between the CD48 high and low groups. Expression of immune checkpoint molecules (CD274, CTLA4, LAG3, TIGIT, PDCD1, HAVCR2) was compared between the two groups. Genes were ranked by Spearman correlation with

CD48 expression, and GSEA [12] (with GO biological process and hallmark gene sets) was used to probe biological pathway differences between the groups. The TIDE (Tumor Immune Dysfunction and Exclusion) algorithm was applied to compute the TIDE score and immune-escape-related scores for T-cell dysfunction, T-cell exclusion, CD8, interferon gamma (IFNG), and CD274 (PD-L1), which were then compared between the CD48 high and low groups.

2.6 Single-Cell Processing and Downstream Analysis

GSE168652 was processed with Seurat [13] (v5.0) using normalization (LogNormalize), highly variable gene identification (vst, top 3,000), scaling, PCA (top 50 principal components), clustering (FindClusters, resolution 1.2), and UMAP embedding. Automatic cell annotation was performed with SingleR [14] against the BlueprintEncodeData reference from the celldex package (259 samples, 43 cell types, built from purified-cell bulk RNA-seq of the Blueprint and ENCODE projects), and epithelial/tumor cells were separately identified by EPCAM expression (log-normalized > 1). Downstream single-cell analyses included Slingshot [15] for pseudotime trajectory inference, CytoTRACE [16] for stemness estimation, AUCell [17] for CD48 gene-set activity, and CellChat [18] for cell-cell communication inference (up to 800 cells randomly sampled per cell type). The CIBERSORTx online platform (https://cibersortx.stanford.edu/) was used with a reference built from cell-subtype-specific gene expression profiles derived from our scRNA-seq data to quantify the relative proportions of cell types in each bulk sample.

2.7 Drug Sensitivity and Somatic Mutations

Drug sensitivity was predicted at the transcriptome level with oncoPredict [19] using the Genomics of Drug Sensitivity in Cancer (GDSC2) reference, and estimated IC50 values for common cervical cancer chemotherapeutics (cisplatin, paclitaxel, gemcitabine, docetaxel, 5-fluorouracil, and others) were compared between the CD48 high and low groups. Somatic mutation (MAF) data of TCGA-CESC were summarized and compared with maftools, and mutation frequencies were contrasted between the CD48 high and low groups. These analyses aim to generate hypotheses for treatment rather than to establish clinical drug response.

2.8 CD48 Virtual Knockout Analysis

Virtual knockout of CD48 in immune cell subsets was performed with scTenifoldKnk [20]. A wild-type gene regulatory network was constructed, and CD48-associated edge weights were set to zero to generate the knockout network. Manifold alignment was used to compare the two networks and compute per-gene projection distances (d-value) and z-scores. Significantly perturbed genes (z-score > 0, $p < 0.05$, log2FC > 2) were then subjected to functional enrichment to infer potential downstream regulatory functions of CD48.

2.9 Statistical Analysis

Continuous variables were compared between groups with the Wilcoxon rank-sum test, multiple groups with the Kruskal-Wallis test, and categorical variables with the chi-

square test. Correlations were assessed by Spearman rank correlation, and survival analyses were performed with the survival package. All analyses were carried out in R (version 4.6.1), and two-sided $p < 0.05$ was considered statistically significant.

3. Results

3.1 Identification of Immune-Related Cervical Cancer Targets (IRCTs)

A scale-free gene co-expression network was built from the xCell ImmuneScore of the TCGA-CESC cohort (296 samples; clinicopathological characteristics in Table S11), and dynamic tree cutting identified six co-expression modules. Module-trait analysis showed that the blue module correlated most strongly with ImmuneScore and was designated the core immune-related module, containing 1,165 genes (Figure 1). Intersecting the blue module with CTD (12 genes) and GeneCards (6,661 genes) targets yielded 364 immune-related cervical cancer targets (IRCTs; Table S1). KEGG enrichment showed that IRCTs were significantly enriched in cytokine-cytokine receptor interaction, viral protein interaction with cytokine and cytokine receptor, hematopoietic cell lineage, Th17 cell differentiation, allograft rejection, graft-versus-host disease, and cell adhesion molecule (CAM) interaction pathways. GO enrichment highlighted regulation of lymphocyte activation, positive regulation of leukocyte activation, regulation of T-cell activation, and leukocyte cell-cell adhesion (Table S2). These pathways are consistent with immune regulation and microenvironment remodeling in cervical cancer.

3.2 Selection of the Core Gene CD48

A co-expression network of IRCTs was built from the TOM and exported to Cytoscape for topology analysis. Among the three machine-learning methods, LASSO selected 21 feature genes, random forest (mean decrease in Gini) returned 10 genes with CD48 ranked first, and SVM-RFE returned 10 genes (Figure 2, Table S3). Univariate Cox regression identified 127 prognostic genes among the 364 IRCTs ($p < 0.05$; Table S4). Intersecting the Cox-significant genes with the LASSO and random forest outputs produced four consensus core genes: CD48, CTLA4, HAVCR2, and CD86, all of which are immune checkpoint or costimulatory molecules. Because CD48 ranked first by random forest importance and was significantly associated with prognosis, it was chosen as the core target for further analysis.

3.3 Expression and Prognostic Significance of CD48

Expression differences were examined in two independent GEO cohorts. In GSE63514 (24 normal, 104 tumor), CD48 was slightly higher in tumor tissue than in normal tissue ($p = 0.079$); GSE39001 (12 normal, 43 tumor) showed a similar trend ($p = 0.474$), but neither reached statistical significance. This indicates that the clinical relevance of CD48 lies in intratumoral immune heterogeneity rather than in overall differences between tumor and normal tissue, consistent with its identity as an immune cell marker whose expression tracks immune infiltration (Figure 3A, B).

In TCGA-CESC, Kaplan-Meier analysis showed that the CD48 high group had significantly longer OS than the low group (log-rank $p = 0.002$), identifying CD48 as a protective factor (Figure 3D). Univariate Cox regression confirmed this protective role (HR = 0.488, 95% CI 0.299–0.795, $p = 0.004$). After adjusting for age, FIGO stage, and

histological subtype, CD48 remained an independent protective factor (HR = 0.498, 95% CI 0.302–0.822, p = 0.006), whereas FIGO stage IV was an independent risk factor (HR = 3.529, 95% CI 1.877–6.636, p < 0.001) (Figure 3C, Table S5).

Time-dependent ROC analysis gave 1-, 3-, and 5-year AUCs of 0.688, 0.616, and 0.622 for CD48 (Figure 3E); the multi-gene risk score model built from the four consensus core genes yielded AUCs of 0.681, 0.625, and 0.623. A nomogram incorporating CD48 expression, age, FIGO stage, and histological subtype was constructed to predict individual 1-, 3-, and 5-year survival probabilities (Figure 3F). Clinical association analysis showed that CD48 expression did not differ across FIGO stages but was markedly elevated in squamous cell carcinoma relative to adenocarcinoma (p < 0.001) (Figure 3H, I). The expression of the consensus checkpoint genes across CD48 groups and clinical features is shown as a heatmap (Figure 3G).

3.4 Association of CD48 with the Immune Microenvironment

After median-based grouping, xCell analysis showed that the CD48 high group had significantly elevated ImmuneScore and increased infiltration of plasma cells, NK cells, monocytes, dendritic cells (DC), and plasmacytoid dendritic cells (pDC) (all p < 0.05). Multiple immune checkpoint molecules, including CD274 (PD-L1), CTLA4, LAG3, TIGIT, PDCD1 (PD-1), and HAVCR2 (TIM-3), were significantly upregulated in the CD48 high group (all p < 0.001) (Figure 4A–C, Table S6). GSEA showed that the CD48 high group was enriched for immune-related biological processes (B-cell receptor signaling, NK-cell activation, T-cell receptor signaling, and antigen processing and presentation), whereas the low group was enriched for metabolic and biosynthetic

processes (GPI-anchor biosynthesis, cholesterol/isoprenoid biosynthesis, and mitochondrial RNA metabolism) (Figure 4D). These results indicate that high CD48 expression marks an immune-activated rather than a purely proliferative cervical cancer phenotype.

We next used TIDE to assess immune-escape features and immunotherapy response potential between the two groups. The TIDE score did not differ significantly between the CD48 high and low groups ($p = 0.260$), suggesting that CD48 expression alone is not a reliable predictor of immunotherapy response. However, the CD48 high group displayed elevated CD8, IFNG, and CD274 (PD-L1) scores together with a reduced T-cell exclusion score (all $p < 0.001$), supporting a "hotter" immune microenvironment. Notably, the CD48 high group also showed a higher T-cell dysfunction score ($p < 0.001$), indicating that this "hot tumor" phenotype coexists with a degree of T-cell dysfunction (Figure 4E, Table S7).

3.5 Single-Cell Expression and Differentiation Dynamics of CD48

Seurat clustering of GSE168652 (24,498 cells) identified 23 subclusters by UMAP, annotated as epithelial/tumor cells, fibroblasts, endothelial cells, CD8+ T cells, NK cells, monocytes, macrophages, CD4+ T cells, B cells, and dendritic cells. CD48 expression was markedly heterogeneous and concentrated in immune subsets (CD8+ T cells, NK cells, monocytes/macrophages), with almost no expression in epithelial/tumor cells; the overall detection rate was below 2%, consistent with its identity as an immune cell marker (Figure 5A, B). Slingshot trajectory inference combined with CytoTRACE stemness estimation delineated the differentiation lineages in the microenvironment, and

AUCell analysis showed that CD48 gene-set activity was concentrated in immune subsets and near zero in non-immune cells such as epithelial, fibroblast, and endothelial cells (Figure 5C–H).

3.6 CD48-Related Cell Communication and Cellular Composition

CellChat revealed the ligand-receptor interaction network among cell types in the cervical cancer microenvironment and identified key pathways mediating intercellular signaling. Because CD48 is expressed mainly in immune cells, communication among immune subsets constitutes the structural basis of its function (Figure 5I). CIBERSORTx deconvolution showed a higher immune cell fraction in CD48 high samples, further supporting the link between CD48 expression and immune-microenvironment remodeling.

3.7 CD48 and Drug Sensitivity

Drug sensitivity prediction showed that, among common cervical cancer chemotherapeutics, the CD48 high group showed markedly lower estimated IC50 values for cisplatin, paclitaxel, gemcitabine, docetaxel, and 5-fluorouracil than the low group (all $p < 0.001$) (Figure 6A, Table S8), suggesting that CD48 high cervical cancers may be more sensitive to these agents. This observation is consistent with the prognostic role of CD48 and may reflect tumor chemosensitivity. However, because these predictions derive from transcriptome-based pharmacogenomic modeling, they should be regarded as hypothesis-generating and interpreted with caution.

3.8 Somatic Mutation Profile Associated with CD48

TCGA-CESC somatic mutations were dominated by missense variants, with frequent mutations in TTN, PIK3CA, MUC16, KMT2C, and KMT2D; PIK3CA is an established driver gene in cervical cancer (Figure 6B). Comparing mutation frequencies between the CD48 high and low groups, HLA-B, SMG1, and EPHA2 were mutated significantly more often in the CD48 high group ($p < 0.05$), with the most pronounced difference in HLA-B, which encodes an MHC class I molecule involved in antigen presentation ($p < 0.001$) (Figure 6C, Table S10). CD48 expression may therefore be associated with distinct molecular subtypes and immune-related mutation backgrounds in cervical cancer.

3.9 Downstream Regulatory Network after CD48 Knockout

scTenifoldKnk virtual knockout was performed on immune cell subsets (622 immune cells, 457 retained after quality control for modeling; 1,991 genes × 457 cells, CD48 detection rate 38.95%). Knockout of CD48 significantly perturbed three genes (FDR < 0.05). Besides CD48 itself, the most perturbed genes were NKG7 and GZMA (z-scores 3.76 and 3.71; FDR 2.21×10^{-10} and 8.88×10^{-9}) (Figure 6D, Table S9), both of which are effector molecules of CD8+ T cells and NK cells (NKG7 mediates granule-mediated cytotoxicity; GZMA is granzyme A). This suggests that the CD48 regulatory network is closely tied to immune effector function, and that CD48 loss primarily perturbs the antitumor effector program mediated by CD8+ T cells and NK cells, supporting a role for CD48 in antitumor immunity in cervical cancer.

4. Discussion

Cervical cancer is driven by persistent HPV infection. Although immune checkpoint inhibitors are approved for recurrent or metastatic disease, only a subset of patients derives durable benefit, and whether immune checkpoint molecule expression can guide prognosis and response prediction remains unsettled. Earlier prognostic studies in cervical cancer focused mostly on molecular alterations within tumor cells, paying less attention to costimulatory or coinhibitory receptors on immune cells, which control effector cell activation and exhaustion. Here we integrated TCGA-CESC bulk and GSE168652 single-cell transcriptomes to evaluate the expression, prognostic value, and immune-microenvironment associations of the immune cell marker CD48.

The main findings are as follows. First, CD48 was consistently prioritized as the consensus core gene by WGCNA, LASSO, random forest, and SVM-RFE, and its high expression correlated with longer cervical cancer survival (log-rank $p = 0.002$). It remained an independent protective factor after adjusting for age, FIGO stage, and histological subtype (HR = 0.498, 95% CI 0.302–0.822, $p = 0.006$). Second, high CD48 coincided with elevated immune scores, increased infiltration of plasma cells, NK cells, monocytes, DCs, and pDCs, and upregulation of several checkpoint molecules, marking an immune-activated microenvironment. Third, at single-cell level CD48 expression was almost entirely confined to CD8+ T cells, NK cells, and monocytes/macrophages and was nearly absent from epithelial/tumor cells (overall detection rate < 2%), so its expression reflects immune cell infiltration rather than the tumor cells themselves. Fourth, virtual knockout of CD48 produced the most significant network perturbation in the cytotoxic

effectors NKG7 and GZMA ($z = 3.76$ and 3.71; FDR = 2.21×10^{-10} and 8.88×10^{-9}), pointing to a regulatory network tied to immune effector function. Fifth, TIDE analysis found no significant difference in the total TIDE score between the CD48 high and low groups ($p = 0.260$), but the high group showed higher CD8, IFNG, and PD-L1 scores and lower exclusion, corresponding to a hotter immune microenvironment.

These results converge on one interpretation: CD48 expression in cervical cancer reflects the degree of effector immune cell infiltration in the tumor microenvironment rather than the malignant phenotype of the tumor epithelium. Single-cell data support this, as CD48 is nearly silent in tumor epithelium but highly expressed in cytotoxic cells such as NK and CD8+ T cells; its protective value (HR = 0.498) corresponds to an immune-activated state with abundant infiltration and preserved effector function. The lack of significant CD48 differences between tumor and normal tissue in the two GEO cohorts ($p = 0.079$ and 0.474) further indicates that the clinical relevance of CD48 stems from intratumoral immune heterogeneity rather than from overall tumor-versus-normal differences. High CD48 also coincided with upregulation of several checkpoint molecules (PD-L1, CTLA4, LAG3, TIGIT), matching the coexistence of activating and inhibitory signals typical of immunologically hot tumors. Given that macrophage polarization and checkpoint signaling both contribute to immune escape in cervical cancer, high CD48 may mark a state with altered immune regulation that in turn affects treatment response. These conclusions nonetheless derive from transcriptome-level computational inference, and the extent to which CD48 shapes these immune phenotypes requires direct experimental confirmation.

CD48 is a SLAM family member and the natural ligand of CD2, and earlier work has focused on its roles in lymphocyte activation and hematological diseases [6]. Placing CD48 in the setting of solid cervical cancer, we found that its expression pattern and prognostic direction align with its immunological function. High CD48 accompanies CD8+ T and NK infiltration and immune activation, and virtual knockout downregulates NKG7 and GZMA, suggesting that CD48 helps maintain effector cell cytotoxicity. This is consistent with its reported costimulatory role and with the T-cell dysfunction caused by its deficiency [6]. In TIDE analysis the CD48 high group paradoxically showed a higher dysfunction score, which can be explained by T-cell exhaustion: under high CTL infiltration, effector cells that receive persistent antigen stimulation simultaneously engage exhaustion programs, so inflammation and exhaustion coexist. CD48 can thus be viewed as a marker reflecting the balance between immune activation and exhaustion, rather than simply another prognosis-associated gene.

At the single-cell level, CD48 is nearly absent from epithelial/tumor cells but highly enriched in CD8+ T cells, NK cells, and monocytes/macrophages, with an overall detection rate below 2%. AUCell analysis likewise localized CD48 gene-set activity to immune subsets, with near-zero activity in epithelial, fibroblast, and endothelial cells; Slingshot pseudotime and CytoTRACE stemness estimation further delineated the differentiation lineages. These observations indicate that CD48 acts chiefly as a microenvironment-associated marker rather than a lineage-specific regulator of cervical epithelial differentiation. CIBERSORTx deconvolution also showed a higher immune cell fraction in CD48 high samples, supporting the association between CD48 expression and microenvironment remodeling. The prognostic significance of CD48 may therefore

originate from the highly infiltrated immune state it marks rather than from intrinsic tumor cell properties.

CellChat analysis revealed extensive ligand-receptor interaction networks among cell types in the cervical cancer microenvironment, and the concentration of CD48 in immune cells suggests that communication among immune subsets forms the structural basis of its function. As a ligand of CD2 and CD244 (2B4), CD48-mediated signaling may relate to the activation and exhaustion states of effector cells. These findings rest on computational ligand-receptor models and should be regarded as preliminary; functional perturbation and spatially resolved experiments will be needed to confirm whether CD48 genuinely participates in these communication changes.

Drug sensitivity prediction offers a translational reference for CD48. The CD48 high group displayed substantially lower predicted IC50 values for cisplatin, paclitaxel, gemcitabine, docetaxel, and 5-fluorouracil (all $p < 0.001$), suggesting that high-expression patients may be more sensitive to these agents. This prediction framework nonetheless rests on GDSC2 transcriptome-based pharmacogenomic modeling rather than a prospective treatment cohort, so it should be treated as a lead whose translational value awaits in vitro and in vivo validation. For mutations, HLA-B, SMG1, and EPHA2 were mutated more frequently in the CD48 high group, with the largest difference in HLA-B, which encodes an MHC class I molecule involved in antigen presentation ($p < 0.001$), suggesting that CD48 expression may relate to distinct molecular subtypes and immune-related mutation backgrounds.

Beyond its value as a marker, CD48 and its SLAM/CD2–CD244 signaling axis could also become a therapeutic target. The association of high CD48 with checkpoint

upregulation, inflammatory activity, and intercellular communication suggests that interventions targeting CD48 might influence both the immune state of the microenvironment and effector cell function; whether blocking the CD48–2B4 axis can reverse NK/CD8+ T-cell exhaustion and cooperate with PD-1/PD-L1 blockade to strengthen antitumor immunity warrants further exploration. These proposals all derive from computational analyses, and their actual therapeutic value requires pharmacological and mechanistic evaluation.

This study has several limitations. All conclusions come from retrospective computational analyses of public data; immune infiltration, cell communication, drug sensitivity, and virtual knockout are computational inferences that lack experimental validation. The single-cell data include only two samples, which may limit the generalizability of conclusions about cellular heterogeneity. The associations between CD48 and prognosis or the immune microenvironment are observational and do not establish a causal, driving role; CD48 may be a marker that tracks immune activation rather than an upstream regulator. Future work could use CD48 knockdown and overexpression, together with gain- and loss-of-function experiments, to clarify its causal role; validate its prognostic and predictive value in multicenter prospective cohorts; and test its potential as a stratification marker in real-world cohorts treated with combination immunotherapy.

5. Conclusions

This study identified CD48 as a consensus core gene in cervical cancer by integrating bulk and single-cell transcriptomic data. High CD48 expression was an independent favorable prognostic factor (HR = 0.498, 95% CI 0.302–0.822, p = 0.006) and marked an immune-activated microenvironment characterized by CD8+ T-cell and NK-cell infiltration, elevated immune checkpoint expression, and higher immune and TIDE-related inflammatory scores. Single-cell analysis localized CD48 expression mainly to CD8+ T cells, NK cells, and monocytes/macrophages rather than tumor epithelium, and virtual knockout of CD48 downregulated the cytotoxic effectors NKG7 and GZMA. These findings support CD48 as an immune-activation marker reflecting effector-cell infiltration, with potential value as a prognostic biomarker and as a therapeutic lead through the CD48–2B4 axis. Because all results derive from retrospective computational analyses, the causal role of CD48 and its utility in immunotherapy stratification require validation by functional experiments and prospective cohorts.

Institutional Review Board Statement

This study was based exclusively on publicly available, de-identified datasets (TCGA and GEO) and did not involve direct interaction with human participants or animals. Therefore, institutional review board approval and informed consent were not required for this study.

Consent to participate

Not applicable.

Consent to publish

Not applicable.

Data Availability Statement

The datasets analyzed in this study are publicly available. Bulk RNA-sequencing data were obtained from The Cancer Genome Atlas (TCGA-CESC, https://portal.gdc.cancer.gov/), and single-cell RNA-sequencing data were obtained from the Gene Expression Omnibus (GEO, accession number GSE168652, https://www.ncbi.nlm.nih.gov/geo/query/acc.cgi?acc=GSE168652).

References

[1] E.M. Burd, Human papillomavirus and cervical cancer, Clin Microbiol Rev 16(1) (2003) 1-17.

[2] E. Wloszek, K. Krupa, E. Skrok, M.P. Budzik, A. Deptala, A. Badowska-Kozakiewicz, HPV and Cervical Cancer-Biology, Prevention, and Treatment Updates, Curr Oncol 32(3) (2025).

[3] Y. Li, J. Deng, Y. Liu, S. Yu, HPV infection and the immune microenvironment in cervical cancer, Front Immunol 16 (2025) 1645019.

[4] X. Chen, Y. Hao, Y. Liu, S. Zhong, Y. You, K. Ao, T. Chong, X. Luo, M. Yin, M. Ye, H. He, A. Lu, J. Chen, X. Li, J. Zhang, X. Guo, NAT10/ac4C/FOXP1 Promotes Malignant Progression and Facilitates Immunosuppression by Reprogramming Glycolytic Metabolism in Cervical Cancer, Adv Sci (Weinh) 10(32) (2023) e2302705.

[5] D. Wang, S. Wu, J. He, L. Sun, H. Zhu, Y. Zhang, S. Liu, X. Duan, Y. Wang, T. Xu, FAT4 overexpression promotes antitumor immunity by regulating the beta-catenin/STT3/PD-L1 axis in cervical cancer, J Exp Clin Cancer Res 42(1) (2023) 222.

[6] S.L. McArdel, C. Terhorst, A.H. Sharpe, Roles of CD48 in regulating immunity and tolerance, Clin Immunol 164 (2016) 10-20.

[7] Z. Lin, Z. Chen, Z. Deng, T. Bao, S. Shen, Dual Regulatory Functions and Therapeutic Potential of CD48 in Tumor Immunity, Oncol Res 34(8) (2026) 11.

[8] D. Aran, Z. Hu, A.J. Butte, xCell: digitally portraying the tissue cellular heterogeneity landscape, Genome Biol 18(1) (2017) 220.

[9] P. Langfelder, S. Horvath, WGCNA: an R package for weighted correlation network analysis, BMC Bioinformatics 9 (2008) 559.

[10] W.G. Touw, J.R. Bayjanov, L. Overmars, L. Backus, J. Boekhorst, M. Wels, S.A. van Hijum, Data mining in the Life Sciences with Random Forest: a walk in the park or lost in the jungle?, Brief Bioinform 14(3) (2013) 315-26.

[11] H. Sanz, C. Valim, E. Vegas, J.M. Oller, F. Reverter, SVM-RFE: selection and visualization of the most relevant features through non-linear kernels, BMC Bioinformatics 19(1) (2018) 432.

[12] A. Subramanian, P. Tamayo, V.K. Mootha, S. Mukherjee, B.L. Ebert, M.A. Gillette, A. Paulovich, S.L. Pomeroy, T.R. Golub, E.S. Lander, J.P. Mesirov, Gene set enrichment analysis: a knowledge-based approach for interpreting genome-wide expression profiles, Proc Natl Acad Sci U S A 102(43) (2005) 15545-50.

[13] A. Butler, P. Hoffman, P. Smibert, E. Papalexi, R. Satija, Integrating single-cell transcriptomic data across different conditions, technologies, and species, Nat Biotechnol 36(5) (2018) 411-420.

[14] D. Aran, A.P. Looney, L. Liu, E. Wu, V. Fong, A. Hsu, S. Chak, R.P. Naikawadi, P.J. Wolters, A.R. Abate, A.J. Butte, M. Bhattacharya, Reference-based analysis of lung single-cell sequencing reveals a transitional profibrotic macrophage, Nat Immunol 20(2) (2019) 163-172.

[15] K. Street, D. Risso, R.B. Fletcher, D. Das, J. Ngai, N. Yosef, E. Purdom, S. Dudoit, Slingshot: cell lineage and pseudotime inference for single-cell transcriptomics, BMC Genomics 19(1) (2018) 477.

[16] G.S. Gulati, S.S. Sikandar, D.J. Wesche, A. Manjunath, A. Bharadwaj, M.J. Berger, F. Ilagan, A.H. Kuo, R.W. Hsieh, S. Cai, M. Zabala, F.A. Scheeren, N.A. Lobo, D. Qian, F.B. Yu, F.M. Dirbas, M.F. Clarke, A.M. Newman, Single-cell transcriptional diversity is a hallmark of developmental potential, Science 367(6476) (2020) 405-411.

[17] S. Aibar, C.B. Gonzalez-Blas, T. Moerman, V.A. Huynh-Thu, H. Imrichova, G. Hulselmans, F. Rambow, J.C. Marine, P. Geurts, J. Aerts, J. van den Oord, Z.K. Atak, J. Wouters, S. Aerts, SCENIC: single-cell regulatory network inference and clustering, Nat Methods 14(11) (2017) 1083-1086.

[18] S. Jin, M.V. Plikus, Q. Nie, CellChat for systematic analysis of cell-cell communication from single-cell transcriptomics, Nat Protoc 20(1) (2025) 180-219.

[19] D. Maeser, R.F. Gruener, R.S. Huang, oncoPredict: an R package for predicting in vivo or cancer patient drug response and biomarkers from cell line screening data, Brief Bioinform 22(6) (2021).

[20] D. Osorio, Y. Zhong, G. Li, Q. Xu, Y. Yang, Y. Tian, R.S. Chapkin, J.Z. Huang, J.J. Cai, scTenifoldKnk: An efficient virtual knockout tool for gene function predictions via single-cell gene regulatory network perturbation, Patterns (N Y) 3(3) (2022) 100434.

[21] J. Galon, D. Bruni, Approaches to treat immune hot, altered and cold tumours with combination immunotherapies, Nat Rev Drug Discov 18(3) (2019) 197-218.

[22] E.J. Wherry, M. Kurachi, Molecular and cellular insights into T cell exhaustion, Nat Rev Immunol 15(8) (2015) 486-99.

Figure Legends

Figure 1. Identification of immune-related cervical cancer targets (IRCTs) by WGCNA. (A) Soft-threshold selection. Left: scale-free topology fit index (R^2) versus soft threshold; right: mean connectivity. The soft threshold $\beta = 6$ was chosen, at which $R^2 > 0.85$ with sufficient network connectivity. (B) Hierarchical clustering dendrogram (based on 1-TOM) of the top 5,000 most variable genes; branch colors indicate WGCNA

co-expression modules. (C) Pearson correlation heatmap between module eigengenes and the xCell ImmuneScore; the MEblue module showed the strongest correlation ($r = 0.85$, $p = 3 \times 10^{-83}$). (D) Venn diagram of the intersection between cervical cancer targets (CTD ∪ GeneCards) and WGCNA module genes, yielding 364 IRCTs. (E) KEGG pathway enrichment of the 364 IRCTs. (F) GO enrichment of the 364 IRCTs (biological process, cellular component, molecular function). CESC, cervical squamous cell carcinoma and endocervical adenocarcinoma.

Figure 2. Identification of the core gene CD48 by integrated machine learning.

(A) LASSO feature selection. Left: binomial deviance versus −log(λ) under 10-fold cross-validation, with the dashed line marking the optimal λ selected by the lambda.1se criterion; right: LASSO coefficient profiles. (B) Random forest gene importance ranking (mean decrease in Gini, top 20 genes shown), with CD48 ranked first. (C) SVM-RFE feature selection (top 10 genes shown). (D) Three-way Venn diagram of univariate Cox-significant genes, LASSO, and random forest outputs, yielding four consensus core genes (CD48, CTLA4, HAVCR2, CD86). (E) Forest plot of univariate Cox regression for prognostic IRCTs (top 20 genes shown; HR and 95% CI on a log scale), with CD48 as a protective factor ($HR < 1$).

Figure 3. Clinical and prognostic significance of CD48.

(A) CD48 expression difference between tumor and normal tissue in GSE63514 ($p = 0.079$). (B) Expression difference in the GSE39001 validation cohort ($p = 0.474$). (C) Multivariate Cox regression forest plot: after adjusting for age, FIGO stage, and histological subtype, CD48 remained an independent protective factor (HR = 0.498, 95% CI 0.302–0.822, $p = 0.006$), and FIGO stage IV was an independent risk factor (HR = 3.529, 95% CI 1.877–6.636). (D) Kaplan-Meier curves of overall survival for CD48 high and low groups in TCGA-CESC (log-rank $p = 0.002$). (E) Time-dependent ROC curves of CD48 for 1-, 3-, and 5-year overall survival (AUC = 0.688, 0.616, and 0.622, respectively). (F) Nomogram incorporating CD48 expression, age, FIGO stage, and histological subtype to predict individual 1-, 3-, and 5-year survival probabilities. (G) Heatmap of consensus core gene and classical immune checkpoint expression across CD48 groups and clinical features (FIGO stage, histological subtype). (H) Distribution of CD48 expression across FIGO stages ($p = 0.35$). (I) Comparison of CD48 expression between adenocarcinoma and squamous cell carcinoma, markedly higher in the latter ($p < 0.001$).

Figure 4. CD48 expression and the immune microenvironment.

(A) Distribution of the xCell ImmuneScore in TCGA-CESC. (B) Comparison of xCell immune cell infiltration scores between the CD48 high and low groups (DC, monocytes, NK cells, pDC, plasma cells; Wilcoxon rank-sum test). (C) Expression of six classical immune checkpoint molecules (CD274, CTLA4, HAVCR2, LAG3, PDCD1, TIGIT) between the two groups (log2(FPKM+1); all $p < 0.0001$, Wilcoxon rank-sum test). (D)

GSEA: the CD48 high group was enriched for immune-related biological processes, and the low group for metabolic and biosynthetic processes (pathways with FDR < 0.05 shown). (E) Immune-escape scores from the official TIDE algorithm (local tidepy implementation): the CD48 high group showed higher CD8, IFNG, and CD274 scores, lower exclusion, and higher dysfunction (all $p < 0.0001$); the total TIDE score did not differ between the groups ($p = 0.260$). n = 296 (148 per group). ns, not significant.

Figure 5. Single-cell atlas and differentiation dynamics of CD48 expression.

(A) UMAP of GSE168652 (24,498 cells): left colored by major cell type, right by tumor versus normal origin. (B) UMAP projection of CD48 expression, enriched in immune subsets. (C) UMAP projection of CD48 gene-set activity computed by AUCell. (D) Violin plots of AUCell scores by cell type: highest in immune subsets and near zero in epithelial, fibroblast, and endothelial cells. (E) UMAP projection of CytoTRACE stemness scores. (F) Violin plots of CytoTRACE scores by cell type. (G) Slingshot pseudotime trajectory reconstruction: left, lineage structure; right, tumor versus normal distribution along the trajectory. (H) Pseudotime ordering. (I) Cell-cell communication network inferred by CellChat (node size reflects signal strength; edges reflect the number of ligand-receptor interactions).

Figure 6. CD48 in relation to therapy-related features and virtual knockout analysis.

(A) Drug sensitivity prediction by oncoPredict with the GDSC2 reference: the CD48 high group had markedly lower estimated IC50 for 5-fluorouracil, cisplatin, docetaxel, gemcitabine, and paclitaxel than the low group (n = 296, 148 per group; Wilcoxon rank-sum test, all $p < 0.0001$). (B) Summary of TCGA-CESC somatic mutations (maftools): missense variants dominated, and C>T transitions were the most frequent SNV class; the most mutated genes included TTN (29%), PIK3CA (28%), MUC16 (17%), KMT2C (15%), and KMT2D (13%). (C) Forest plot of differentially mutated genes between the CD48 high and low groups (Fisher's exact test, minMut = 3, top 12 genes by p value; circles indicate odds ratios and lines the 95% CI; open triangles mark odds ratios beyond the axis range). All top 12 genes were enriched in the CD48 high group, with the largest difference in HLA-B, which encodes an MHC class I molecule (12 vs 0, $p = 1.7 \times 10^{-4}$). (D) Network perturbation fold change (FC) of cytotoxic effectors after scTenifoldKnk virtual knockout of CD48: NKG7 (FC = 53.8, FDR = 2.21×10^{-10}) and GZMA (FC = 45.8, FDR = 8.88×10^{-9}) were most perturbed, whereas PRF1 and GNLY were not significantly perturbed.

Abbreviations

The following abbreviations are used in this manuscript:

AUC: area under the curve

CESC: cervical squamous cell carcinoma and endocervical adenocarcinoma

CI: confidence interval

CIBERSORTx: cell-type identification by estimating relative subsets of RNA transcripts

CTD: Comparative Toxicogenomics Database

CTL: cytotoxic T lymphocyte

DC: dendritic cell

FC: fold change

FDR: false discovery rate

FIGO: International Federation of Gynecology and Obstetrics

FPKM: fragments per kilobase of transcript per million mapped reads

GDSC: Genomics of Drug Sensitivity in Cancer

GEO: Gene Expression Omnibus

GO: Gene Ontology

GPI: glycosylphosphatidylinositol

GSEA: gene set enrichment analysis

HPV: human papillomavirus

HR: hazard ratio

IC50: half-maximal inhibitory concentration

IRCTs: immune-related cervical cancer targets

KEGG: Kyoto Encyclopedia of Genes and Genomes

LASSO: least absolute shrinkage and selection operator

MAF: mutation annotation format

MHC: major histocompatibility complex

NK: natural killer

OS: overall survival

PCA: principal component analysis

RF: random forest

ROC: receiver operating characteristic

scRNA-seq: single-cell RNA sequencing

SLAM: signaling lymphocytic activation molecule

SNV: single-nucleotide variant

SVM-RFE: support vector machine with recursive feature elimination

TCGA: The Cancer Genome Atlas

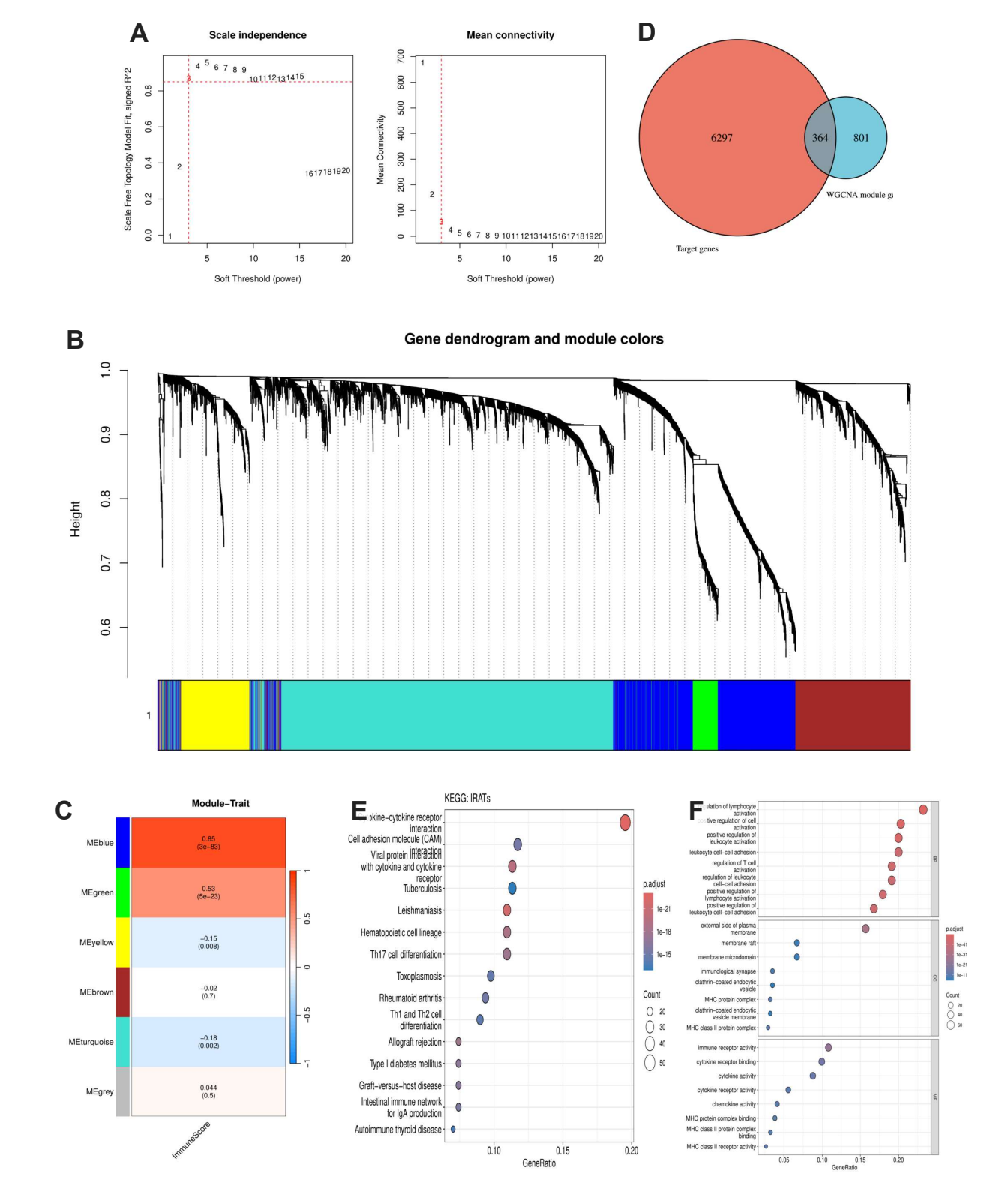
TIDE: tumor immune dysfunction and exclusion

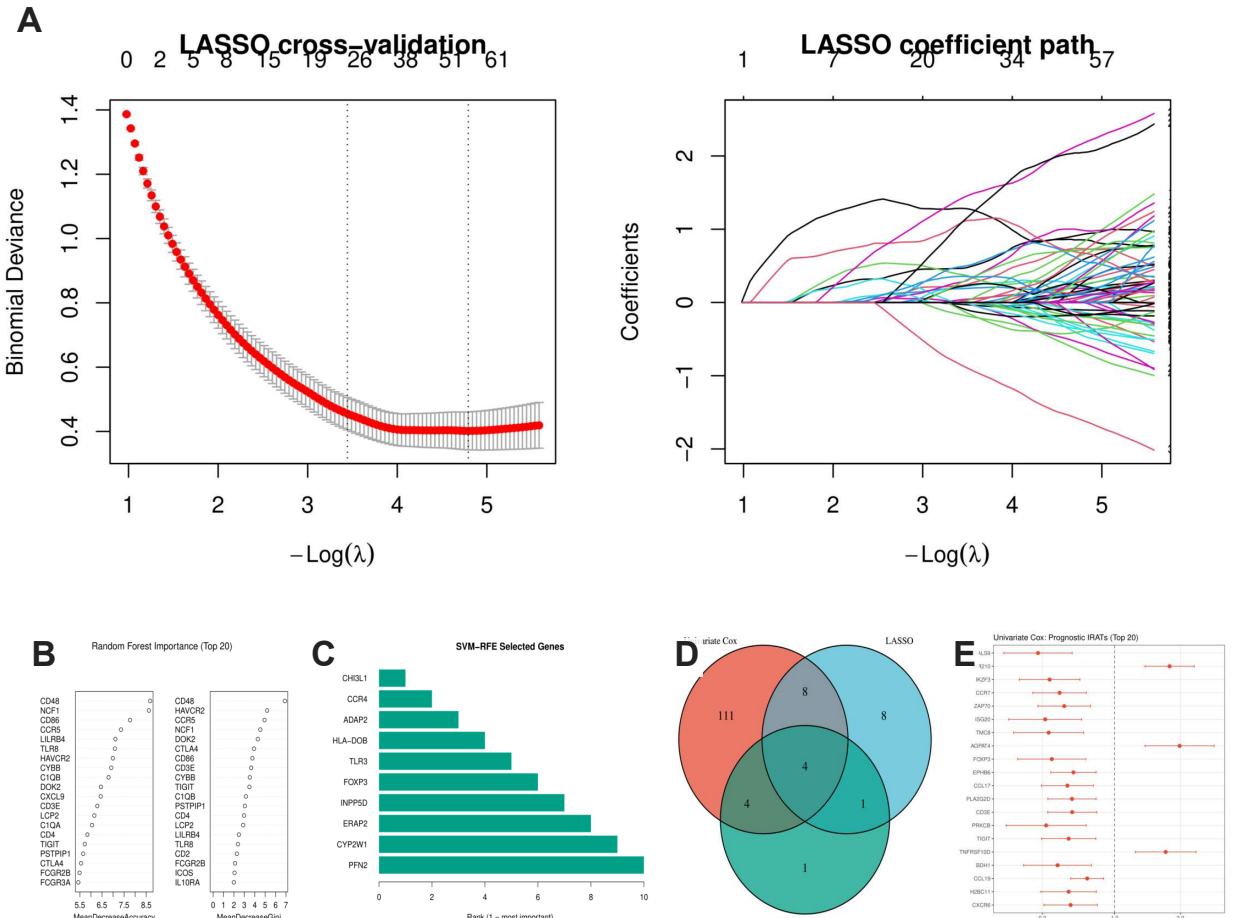
TME: tumor microenvironment

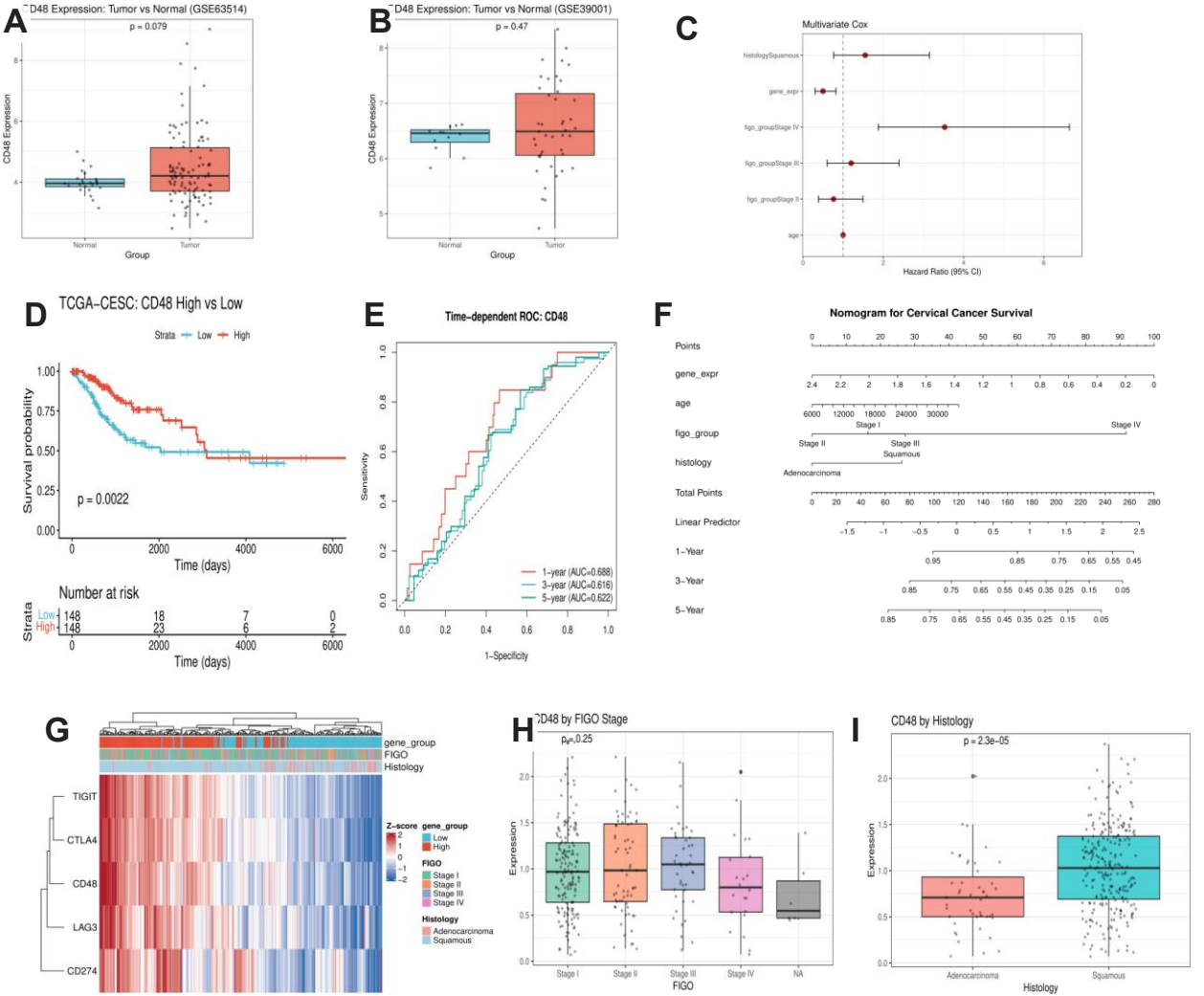
TOM: topological overlap matrix

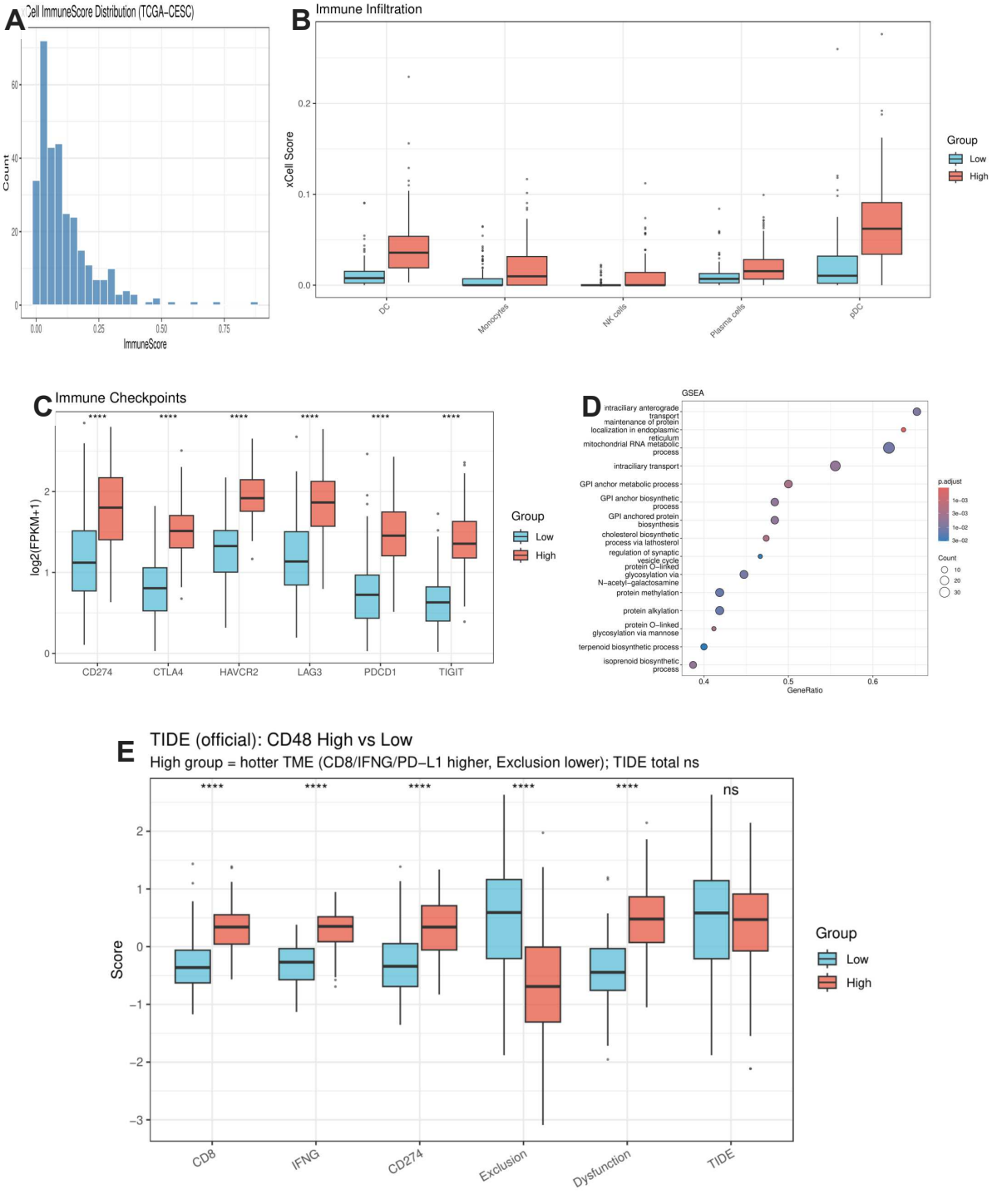
UMAP: uniform manifold approximation and projection

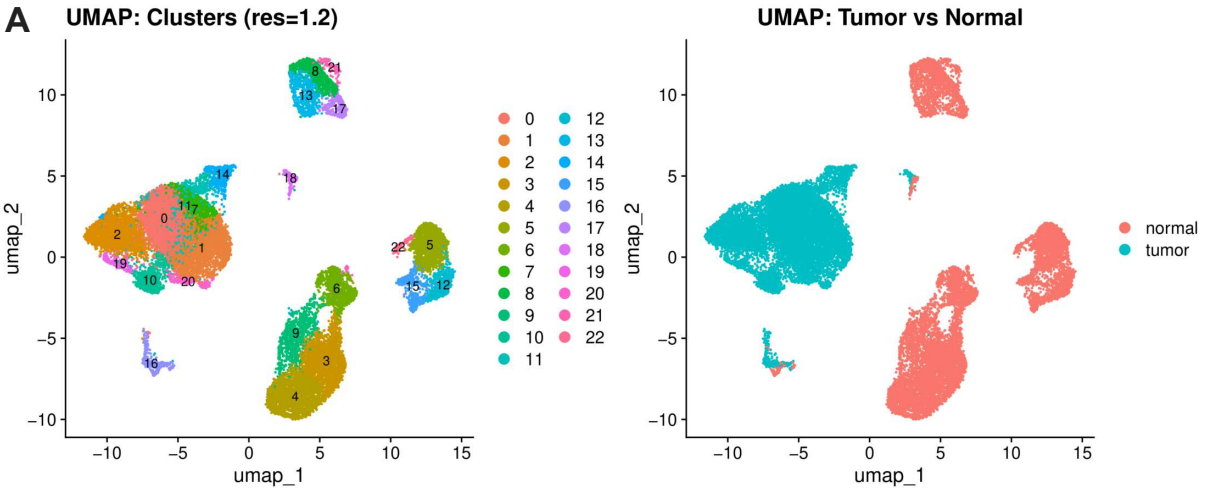
WGCNA: weighted gene co-expression network analysis

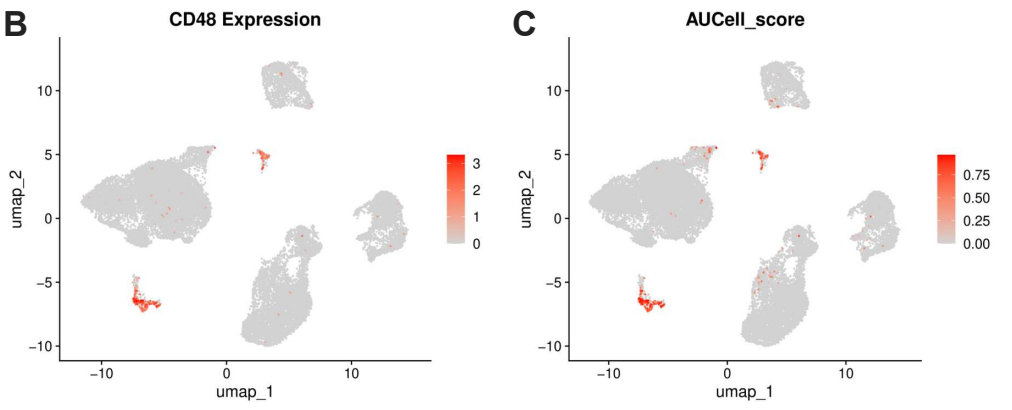

A
Scale independence
Scale Free Topology Model Fit, signed R^2
Soft Threshold (power)
Mean connectivity
Mean Connectivity
Soft Threshold (power)
D
6297
364
801
Target genes
WGCNA module ge
B
Gene dendrogram and module colors
Height
C
Module−Trait
MEblue
MEgreen
MEyellow
MEbrown
MEturquoise
MEgrey
0.85 (3e−83)
0.53 (5e−23)
−0.15 (0.008)
−0.02 (0.7)
−0.18 (0.002)
0.044 (0.5)
ImmuneScore
E
KEGG: IRATs
Cell adhesion molecule (CAM)
Viral protein interaction with cytokine and cytokine receptor
Tuberculosis
Leishmaniasis
Hematopoietic cell lineage
Th17 cell differentiation
Toxoplasmosis
Rheumatoid arthritis
Th1 and Th2 cell differentiation
Allograft rejection
Type I diabetes mellitus
Graft−versus−host disease
Intestinal immune network for IgA production
Autoimmune thyroid disease
GeneRatio
p.adjust
Count
F
positive regulation of leukocyte activation
leukocyte cell−cell adhesion
regulation of T cell activation
regulation of leukocyte cell−cell adhesion
positive regulation of lymphocyte activation
positive regulation of leukocyte cell−cell adhesion
external side of plasma membrane
membrane raft
membrane microdomain
immunological synapse
clathrin−coated endocytic vesicle
MHC protein complex
clathrin−coated endocytic vesicle membrane
MHC class II protein complex
immune receptor activity
cytokine receptor binding
cytokine activity
cytokine receptor activity
chemokine activity
MHC protein complex binding
MHC class II protein complex binding
MHC class II receptor activity
GeneRatio
p.adjust
Count

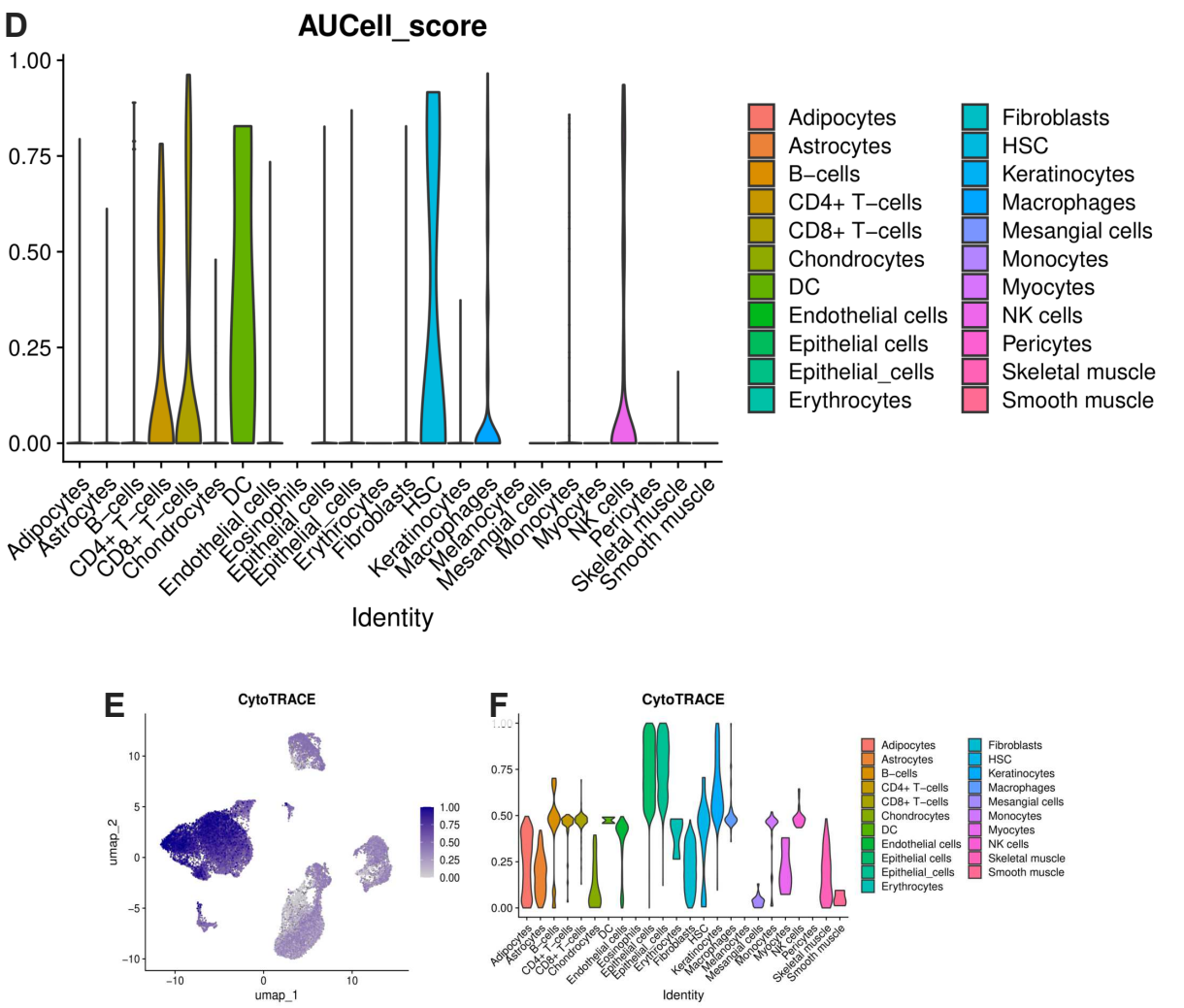

A
LASSO cross-validation
0 2 5 8 15 19 26 38 51 61
Binomial Deviance
0.4 0.6 0.8 1.0 1.2 1.4
1 2 3 4 5
−Log(λ)
LASSO coefficient path
1 7 20 34 57
Coefficients
−2 −1 0 1 2
1 2 3 4 5
−Log(λ)
B
Random Forest Importance (Top 20)
CD48
NCF1
CD86
CCR5
LILRB4
TLR8
HAVCR2
CYBB
C1QB
DOK2
CXCL9
CD3E
LCP2
C1QA
CD4
TIGIT
PSTPIP1
CTLA4
FCGR2B
FCGR3A
5.5 6.5 7.5 8.5
MeanDecreaseAccuracy
CD48
HAVCR2
CCR5
NCF1
DOK2
CTLA4
CD86
CD3E
CYBB
TIGIT
C1QB
PSTPIP1
CD4
LCP2
LILRB4
TLR8
CD2
FCGR2B
ICOS
IL10RA
0 1 2 3 4 5 6 7
MeanDecreaseGini
C
SVM-RFE Selected Genes
CHI3L1
CCR4
ADAP2
HLA-DOB
TLR3
FOXP3
INPP5D
ERAP2
CYP2W1
PFN2
0 2 4 6 8 10
Rank (1 = most important)
D
LASSO
111
8
8
4
4
1
1
Random Forest
E
Univariate Cox: Prognostic IRATs (Top 20)
0.3 1.0 3.0
Hazard Ratio (log10 scale)


A
CD48 Expression: Tumor vs Normal (GSE63514)
p = 0.079
CD48 Expression
Normal
Tumor
Group
B
CD48 Expression: Tumor vs Normal (GSE39001)
p = 0.47
CD48 Expression
Normal
Tumor
Group
C
Multivariate Cox
histologySquamous
gene_expr
figo_groupStage IV
figo_groupStage III
figo_groupStage II
age
Hazard Ratio (95% CI)
D
TCGA-CESC: CD48 High vs Low
Strata Low High
Survival probability
p = 0.0022
Time (days)
Number at risk
Strata
Low 148 18 7 0
High 148 23 6 2
Time (days)
E
Time-dependent ROC: CD48
Sensitivity
1-Specificity
1-year (AUC=0.688)
3-year (AUC=0.616)
5-year (AUC=0.622)
F
Nomogram for Cervical Cancer Survival
Points
gene_expr
age
figo_group
Stage I
Stage II
Stage III
Stage IV
histology
Squamous
Adenocarcinoma
Total Points
Linear Predictor
1-Year
3-Year
5-Year
G
gene_group
FIGO
Histology
TIGIT
CTLA4
CD48
LAG3
CD274
Z-score
gene_group
Low
High
FIGO
Stage I
Stage II
Stage III
Stage IV
Histology
Adenocarcinoma
Squamous
H
CD48 by FIGO Stage
p = 0.25
Expression
Stage I
Stage II
Stage III
Stage IV
NA
FIGO
I
CD48 by Histology
p = 2.3e-05
Expression
Adenocarcinoma
Squamous
Histology

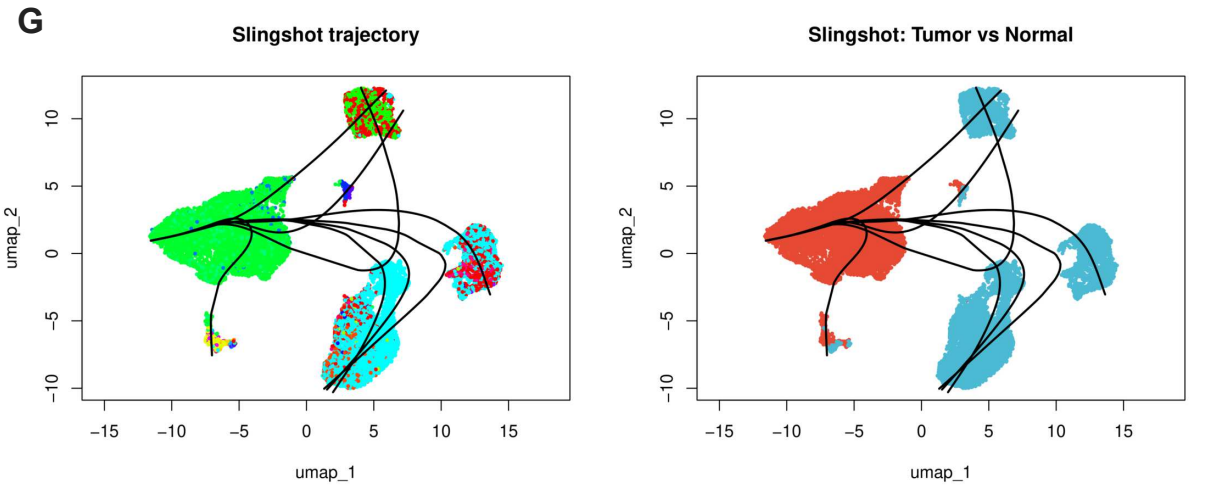

A
Cell ImmuneScore Distribution (TCGA-CESC)
Count
ImmuneScore
B
Immune Infiltration
xCell Score
DC
Monocytes
NK cells
Plasma cells
pDC
Group
Low
High
C
Immune Checkpoints
log2(FPKM+1)
CD274
CTLA4
HAVCR2
LAG3
PDCD1
TIGIT
Group
Low
High
D
GSEA
intraciliary anterograde transport
maintenance of protein localization in endoplasmic reticulum
mitochondrial RNA metabolic process
intraciliary transport
GPI anchor metabolic process
GPI anchor biosynthetic process
GPI anchored protein biosynthesis
cholesterol biosynthetic process via lathosterol
regulation of synaptic vesicle cycle
protein O-linked glycosylation via N-acetyl-galactosamine
protein methylation
protein alkylation
protein O-linked glycosylation via mannose
terpenoid biosynthetic process
isoprenoid biosynthetic process
GeneRatio
p.adjust
Count
E
TIDE (official): CD48 High vs Low
High group = hotter TME (CD8/IFNG/PD-L1 higher, Exclusion lower); TIDE total ns
Score
CD8
IFNG
CD274
Exclusion
Dysfunction
TIDE
ns
Group
Low
High

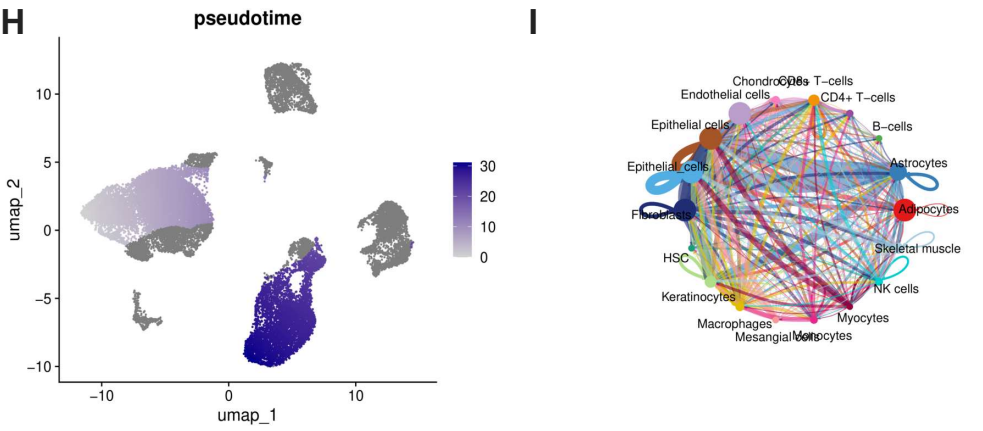

A
UMAP: Clusters (res=1.2)
UMAP: Tumor vs Normal
umap_1
umap_2
normal
tumor

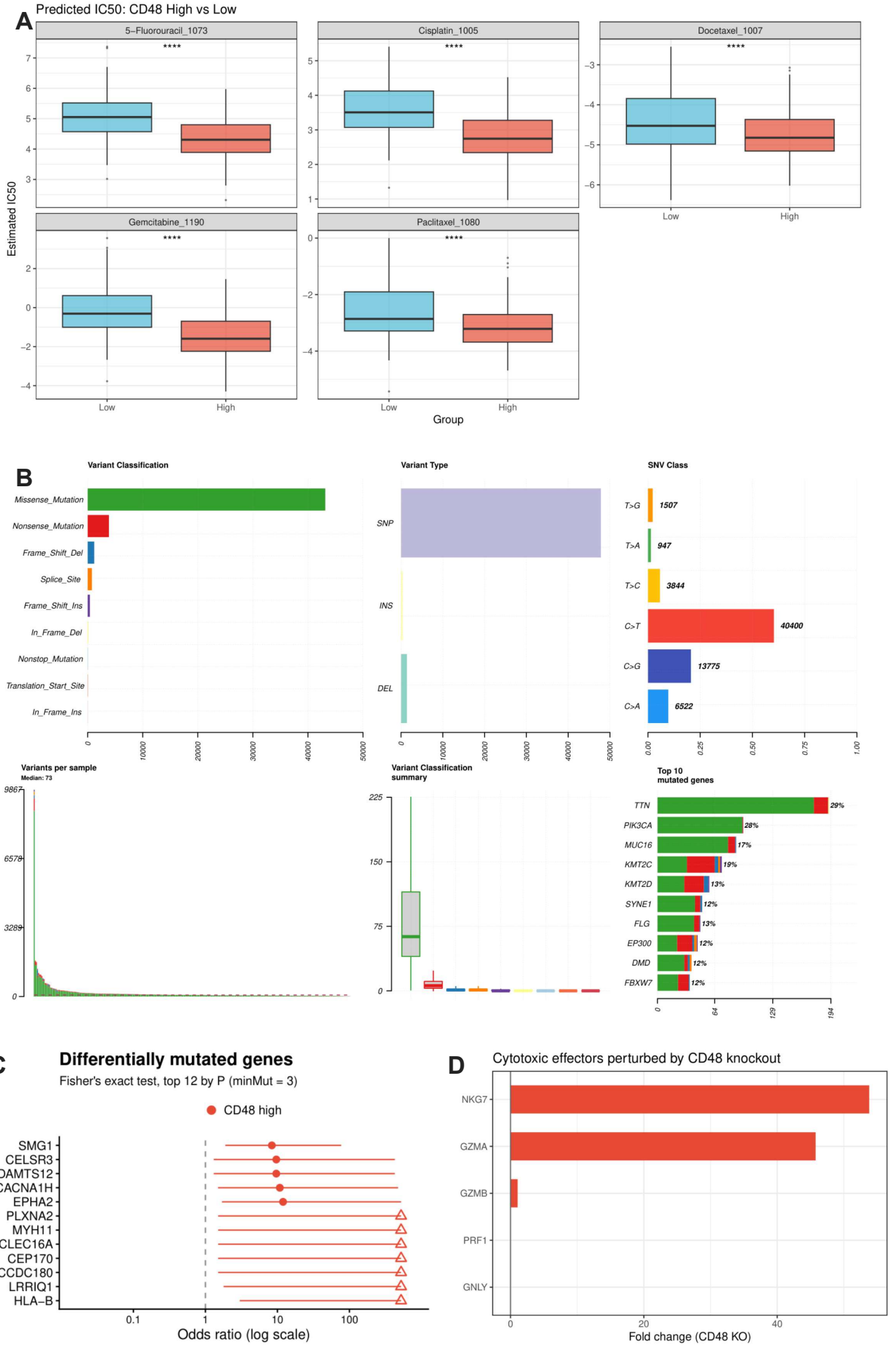

B
CD48 Expression
C
AUCell_score
umap_1
umap_2


D
AUCell_score
Adipocytes
Astrocytes
B−cells
CD4+ T−cells
CD8+ T−cells
Chondrocytes
DC
Endothelial cells
Epithelial cells
Epithelial_cells
Erythrocytes
Fibroblasts
HSC
Keratinocytes
Macrophages
Mesangial cells
Monocytes
Myocytes
NK cells
Pericytes
Skeletal muscle
Smooth muscle
Identity

E
CytoTRACE
F
CytoTRACE
umap_1
umap_2
Identity


G
Slingshot trajectory
Slingshot: Tumor vs Normal
umap_1
umap_2


H
pseudotime
I
umap_1
umap_2


A
Predicted IC50: CD48 High vs Low
5−Fluorouracil_1073
Cisplatin_1005
Docetaxel_1007
Gemcitabine_1190
Paclitaxel_1080
****
Estimated IC50
Low
High
Group
B
Variant Classification
Missense_Mutation
Nonsense_Mutation
Frame_Shift_Del
Splice_Site
Frame_Shift_Ins
In_Frame_Del
Nonstop_Mutation
Translation_Start_Site
In_Frame_Ins
Variant Type
SNP
INS
DEL
SNV Class
T>G 1507
T>A 947
T>C 3844
C>T 40400
C>G 13775
C>A 6522
Variants per sample
Median: 73
Variant Classification summary
Top 10 mutated genes
TTN 29%
PIK3CA 28%
MUC16 17%
KMT2C 19%
KMT2D 13%
SYNE1 12%
FLG 13%
EP300 12%
DMD 12%
FBXW7 12%
C
Differentially mutated genes
Fisher's exact test, top 12 by P (minMut = 3)
CD48 high
SMG1
CELSR3
ADAMTS12
CACNA1H
EPHA2
PLXNA2
MYH11
CLEC16A
CEP170
CCDC180
LRRIQ1
HLA−B
Odds ratio (log scale)
D
Cytotoxic effectors perturbed by CD48 knockout
NKG7
GZMA
GZMB
PRF1
GNLY
Fold change (CD48 KO)

Supplementary Files

This is a list of supplementary files associated with this preprint. Click to download.

- SupplementaryMaterial.docx
- GraphicalAbstract.pdf